



**HAL**  
open science

## Physical Model for Studying the Migration of Fine Particles in the Railway Substructure

Trong Vinh Duong, Yu-Jun Cui, Anh Minh A.M. Tang, Jean Claude Dupla, Jean Canou, Nicolas Calon, Alain Robinet, Baptist Chapot, Emmanuel de Laure

► **To cite this version:**

Trong Vinh Duong, Yu-Jun Cui, Anh Minh A.M. Tang, Jean Claude Dupla, Jean Canou, et al.. Physical Model for Studying the Migration of Fine Particles in the Railway Substructure. Geotechnical Testing Journal, 2014, 37 (5), pp.895-906. 10.1520/GTJ20130145 . hal-01111314

**HAL Id: hal-01111314**

**<https://enpc.hal.science/hal-01111314>**

Submitted on 25 Apr 2018

**HAL** is a multi-disciplinary open access archive for the deposit and dissemination of scientific research documents, whether they are published or not. The documents may come from teaching and research institutions in France or abroad, or from public or private research centers.

L'archive ouverte pluridisciplinaire **HAL**, est destinée au dépôt et à la diffusion de documents scientifiques de niveau recherche, publiés ou non, émanant des établissements d'enseignement et de recherche français ou étrangers, des laboratoires publics ou privés.

1 A physical model for studying the migration of fine particles in railway sub-  
2 structure

3 Duong T.V.<sup>1</sup>, Cui Y.J.<sup>1</sup>, Tang A.M.<sup>1</sup>, Dupla J.C.<sup>1</sup>, Canou J.<sup>1</sup>, Calon N.<sup>2</sup>, Robinet A.<sup>2</sup>, Chabot B.<sup>1</sup>, De  
4 Laure E.<sup>1</sup>

5 <sup>1</sup>: Ecole des Ponts ParisTech, U.R. Navier/CERMES, 6 – 8 av. Blaise Pascal, Cité Descartes,  
6 Champs – sur – Marne, 77455 Marne – la – Vallée cedex 2, France

7 <sup>2</sup>: French Railway Company (SNCF)

8

9

10

11 **Corresponding author:**

12 Prof. Yu-Jun CUI

13 Ecole des Ponts ParisTech

14 6-8 av. Blaise Pascal, Cité Descartes, Champs-sur-Marne

15 F-77455 Marne – la – Vallée cedex - France

16 Telephone: +33 1 64 15 35 50

17 Fax: +33 1 64 15 35 62

18 E-mail : [yujun.cui@enpc.fr](mailto:yujun.cui@enpc.fr)

19

20 ***Abstract***

21 In order to study the creation of interlayer and the mud pumping phenomena in the conventional French  
22 railway substructure, a physical model was developed with a 160 mm thickness ballast layer overlying a  
23 220 mm thickness artificial silt layer (mixture of crushed sand and kaolin), both layers being compacted  
24 in a cylinder of 550 mm inner diameter. One positive pore water pressure sensor, three tensiometers and  
25 three TDR sensors were installed around the ballast/silt interface allowing the evolution of pore water  
26 pressure (negative or positive) and volumetric water content to be monitored, respectively. A digital  
27 camera was installed allowing direct monitoring of different movements (ballast, ballast/sub-soil  
28 interface, etc.). The effects of loading (monotonic and cyclic loadings) and degree of saturation of sub-  
29 soil ( $w = 16\%$ ,  $S_r = 55\%$  and near saturation state) were investigated. It was found that the development  
30 of pore water pressure in the sub-soil is the key factor causing the migration of fine particles that results  
31 in the creation of interlayer as well as the mud pumping. In particular, thanks to the camera, the pumping  
32 up level of fine particles was visualized during the test, showing that the migration of fine particles was  
33 not only due to the interpenetration of ballast particles and sub-soil, but also the pore water pressure that  
34 pushed the fine particle upwards. The relevant results obtained proved that the experimental set-up is  
35 appropriate to be used in investigating the degradation of railway sub-structure.

36

37 *Keywords:* railway substructure; physical model; cyclic loading; pore water pressure; interlayer creation;  
38 mud pumping.

39

40

## 41 **Introduction**

42 Problems related to track settlement and stability come not only from the degradation of each layer but  
43 also from the interaction between layers. Very often, fine particles migration from sub-grade results in  
44 changes of sub-structure components, corresponding to mud pumping or creation of interlayer. Mud  
45 pumping is characterized by the migration of sub-soil fine particles in the ballast layer. It was widely  
46 recognized in both the railway context (Ayres 1986, Selig and Waters 1994, Raymond 1999,  
47 Voottipruex and Roongthanee 2003, Burns et al. 2006, Gataora et al. 2006, Aw 2004, 2007, Indraratna et  
48 al. 2011) and the pavement context (Yoder 1957, Van 1985, Alobaidi and Hoare 1994, 1996, 1998a,  
49 1998b, 1999, Zhang 2004, Yuan et al. 2007). By contrast, the interlayer has been identified and  
50 characterized only recently (Calon et al. 2010, Trinh et al. 2011, Trinh 2011, Trinh et al. 2012, Cui et al.  
51 2013, Duong et al. 2013). This interlayer mainly involves the conventional lines. Indeed, the  
52 conventional lines in France were constructed more than one hundred years ago by directly putting  
53 ballast onto the sub-grade (unlike the new lines for high speed trains). Over years of operation, the  
54 interlayer was formed mainly by the interpenetration between the sub-grade soil and ballast under the  
55 effect of train action. As both mud pumping and presence of interlayer can significantly affect the track  
56 mechanical behavior, it appears important to investigate the related mechanisms in-depth.

57 Up to now, even migration of fine particles and its consequence have been reported in several studies,  
58 the knowledge on the driving mechanisms is still limited. Indeed, in the case of interlayer, its creation is  
59 still an open question. For the mud pumping, some different mechanisms were proposed. Takatoshi  
60 (1997) reported that pumping of fine particles is due to the effect of suction generated by the upward and  
61 downward movement of ties. Differently, Alobaidi and Hoare (1996, 1999) proposed that pumping of  
62 fine particles depends mainly on the pore water pressure developed at the interface between the sub-  
63 grade and sub-base/ballast layer.

64 As far as the experimental work is concerned, few studies have been undertaken in the laboratory.  
65 Alobaidi and Hoare (1996) developed an apparatus from a modified 350 mm triaxial cell. Using this  
66 apparatus, the pumping of fine particles in highway pavement was investigated under 2 Hz loading on a  
67 32 mm diameter metallic hemisphere representing the sub-base material. However, this prototype  
68 apparatus and the adopted methodology are not suitable for the railway issue (metallic hemisphere  
69 instead of ballast, low loading frequency), and in addition, the pumping level of fine particles was only  
70 recorded at the end of the test. Burns et al. (2006) and Ghataora et al. (2006) developed a 230 mm  
71 diameter steel cylinder to test a 200 mm thick sub-grade beneath a 75 mm thick ballast layer. In this  
72 case, the diameter of the cylinder seems to be small when considering the ballast size (about 60 mm).  
73 Moreover, the monitoring of the intermixing of sub-soil particles and ballast particle is also not allowed.

74 In this study, a physical model was developed, allowing the mud pumping and the creation of interlayer  
75 to be investigated. The model had a diameter of 550 mm that is considered as large enough to minimize  
76 any size effect. The apparatus was equipped with 3 tensiometers and 3 time domain reflectometer (TDR)  
77 allowing the monitoring of pore water pressure and volumetric water content at different positions,  
78 respectively. Moreover, a digital camera was used to monitor the evolution of the interface between  
79 ballast and sub-soil. In order to study the creation of interlayer within the sub-structure of conventional  
80 lines in the French railway network, the sample was prepared with a ballast layer overlying a sub-soil  
81 layer. This configuration represents the conventional railway sub-structure at the moment of construction  
82 (more than one hundred years ago). The mud pumping phenomenon was also investigated.

### 83 **Materials**

84 In order to have a quantity of homogeneous sub-soil large enough for conducting the experimental  
85 investigation planned, the sub-soil used in this study was produced artificially by mixing 30% Kaolin  
86 Speswhite clay and 70 % crushed sand C10 (by dry mass). It is named henceforth *70S30K*. The reason of

87 using this artificial material is that it can be reproduced easily in the laboratory for having a large  
88 quantity needed for the whole test program, thus avoiding any problems related to the natural soil  
89 heterogeneity – the composition of soil can be slightly different from one sample to another. Figure 1  
90 shows the grain size distribution curves of Kaolin Speswhite clay, of the crushed sand C10 (given by  
91 suppliers) and of the mixture *70S30K* (determined using the dry sieving and the hydrometer methods).  
92 Note that the curve of *70S30K* is close to that of the Jossigny silt, a soil widely studied worldwide for its  
93 hydro-mechanical behavior especially in the unsaturated state (see Cui and Delage 1996 for instance).  
94 The Standard Proctor curve of *70S30K* is plotted in Figure 2; its hydraulic conductivity at a dry unit  
95 mass of  $1.5 \text{ Mg/m}^3$  is  $8.4 \times 10^{-7} \text{ m/s}$ . Some other properties are presented in Table 1.

96 The ballast used in this study was taken from the storage of construction materials of the French Railway  
97 company (SNCF). It is a granular material with  $d/D = 25/50 \text{ mm}$ . The maximum diameter of ballast is 63  
98 mm. Detailed characteristics of the conventional ballast can be found in SNCF (1995) and Al Shaer  
99 (2005).

## 100 **Experimental setup and procedures**

101 Figure 3 presents schematic views of the physical model including a 3D view (Figure 3a), a side view  
102 (Figure 3b) and a cross section (Figure 3c). The wall of the apparatus was made of Poly(methyl  
103 methacrylate) (PMMA) which is a transparent thermoplastic allowing an external observation by digital  
104 camera. The transparent cell has an internal diameter of 550 mm, a wall thickness of 20 mm and a height  
105 of 600 mm. With these dimensions, any size effect is expected to be minimized as the ratio of the  
106 apparatus diameter to that of ballast particles is larger than 10. Indeed, this ratio is two times the value  
107 recommended by the AFNOR standard (2004) and the values adopted by other authors (Yasuda et al.  
108 1997, Lackenby et al. 2007, Ekblad 2008). The column has different holes that can host 10 tensiometers  
109 and 5 TDRs at different heights. These holes are divided into three groups disposed at  $90^\circ$ ; groups 1 and

110 3 are for the tensiometers and group 2 is for TDRs. Note that during the test when a hole was not used  
111 for sensor installation, it was filled by a special plug having the same dimensions of the hole in order to  
112 not affect the test. In this study, only three volumetric water content sensors (TDR1 to TDR3) and three  
113 tensiometers (T1 to T3) were installed along the column at different heights:  $h = 120, 160$  and  $200$  mm  
114 (the elevation is measured from the bottom of the apparatus). These positions were chosen in order to  
115 have maximum information about the pore water pressure and volumetric water content not only at the  
116 position ( $200$  mm) near the interface between the sub-soil and the ballast but also inside the sub-soil  
117 layer ( $120$  mm). On the top of the PMMA wall, a Light-Emitting Diode (LED) series was installed  
118 lighting up the apparatus wall and thus improving the observation quality by the digital camera. The  
119 PMMA cylindrical wall was fixed on a metallic base plate using screws. A porous plate and a geotextile  
120 were placed at the bottom of the sample to ensure uniform water distribution and to avoid any loss of  
121 soil particles. At the bottom of apparatus ( $h = 0$  mm), a pressure transducer was installed for measuring  
122 the positive pore water pressure in saturated case.

123 For the specimen preparation, crushed sand (C10) and clay (kaolin Speswhite) were mixed up  
124 with water to obtain the target water content - the optimum water content  $w = 16$  % (see Figure 2). After  
125 mixing, the wet material was stored in hermetic containers for at least  $24$  h for moisture homogenization.  
126 The soil specimen was prepared by manual compaction in five layers of  $40$  mm thick each and one layer  
127 of  $20$  mm thick, making a total of  $220$  mm thickness for the whole specimen. In the literature involving  
128 the study on the migration of fine particles, the value of dry unit mass considered is often around  $1.50$   
129  $\text{Mg/m}^3$ :  $1.45 \text{ Mg/m}^3$  in Burns et al. (2006) and from  $1.52$  to  $1.54 \text{ Mg/m}^3$  in Alobaidi et al (1999).  
130 According to Burns et al. (2006), this value corresponds to the medium strength in field conditions.  
131 Thereby, the dry unit mass of  $1.50 \text{ Mg/m}^3$  was chosen in this study. With the specific gravity of clay and  
132 crushed sand (see Table 1), the corresponding porosity and the degree of saturation calculated are  $43\%$   
133 and  $55\%$ , respectively. The TDR probes were installed during the specimen compaction between the

134 sub-layers of sub-soil at the target heights. Once the sub-soil was compacted, 160 mm ballast was placed  
135 on the sub-soil and the ballast particles were arranged in order to have a satisfactory horizontal surface  
136 between ballast and piston. After the specimen preparation, the whole column was placed under the  
137 hydraulic actuator. The tensiometers were then installed, and other operations were undertaken such as  
138 lighting up the LED series, setting up the digital camera, preparing the loading program. Figure 4  
139 presents a photograph of the column with specimen.

140         The test was carried out in three stages. In the first stage (namely henceforth *Unsaturated state*)  
141 where the sub-soil was in unsaturated state ( $w = 16\%$ ;  $S_r = 55\%$ ), a pre-loading (including monotonic  
142 loading and cyclic loading at low frequency) was firstly applied. Monotonic loading started from 0 to  
143 100 kPa at a rate of 0.14 kPa/s. Afterwards, low frequency cyclic loading was applied with the axial  
144 stress varying from 30 to 100 kPa: 20 cycles at 0.1 Hz; 50 cycles at 1Hz and 100 cycles at 2 Hz. This  
145 pre-loading was applied in order to ensure the good functioning of the apparatus before applying a  
146 frequency as high as 5 Hz. The results during this stage are shown in Figure 5. A 5 Hz loading was  
147 applied afterwards for 500 000 cycles. Note that the choice of load amplitude and the frequency was  
148 made based on the consideration of loading conditions in the conventional sub-structure in France (see  
149 Trinh et al. 2012; Duong et al. 2013).

150         Basically, mud pumping is more pronounced when the sub-soil is saturated. For this reason, after  
151 the first stage – *Unsaturated state*, a second stage namely Saturation followed by a third stage namely  
152 *Saturated state* was applied. During the saturation, the sub-soil was saturated from the bottom under a  
153 hydraulic head of 12 kPa using an external water source connected to the column. The water level was  
154 maintained at 2 cm above the ballast/sub-soil interface in order to ensure the fully saturated state of the  
155 sub-soil layer. Meanwhile, a sensor of pore water pressure was installed at  $h = 0$  mm. In *Saturated state*,  
156 monotonic loading at the same increase rate as in *Unsaturated state* was applied up to 100 kPa followed



157 by the 5 Hz cyclic loading. The test ended when fine particles were observed at the surface of ballast  
158 layer.

159 During the test, the variation of pore water pressure was recorded with 3 home-made  
160 tensiometers that are based on the same principle as the high capacity tensiometers developed by Mantho  
161 (2005), Cui et al. (2008), Lourenço et al. (2011) and Toll et al. (2012). The working pressure range of  
162 these tensiometers is from 700 kPa to -700 kPa (they measure both positive pressure and suction). The  
163 time-domain reflectometry (TDR) was connected to a data logger - Trase BE allowing the dielectric  
164 constant  $K_a$  to be recorded, which is deduced from the crossing time of electromagnetic wave within the  
165 surrounding material. The accuracy of the measurement is  $\pm 2\%$ . The well-known model of Topp et al.  
166 (1980) was applied to calculate the volumetric water content:

$$167 \quad \theta = -5.3 \times 10^{-2} + 2.92 \times 10^{-2} K_a - 5.5 \times 10^{-4} K_a^2 + 4.3 \times 10^{-6} K_a^3 \quad (1)$$

## 168 **Experimental results and discussions**

169 Figure 5 presents the results obtained during the pre-loading in *Unsaturated state*. The variation  
170 of stress applied was plotted in Figure 5a where the stress was increased monotonically from 0 to 100  
171 kPa and then cyclically at low frequency before the 5 Hz loading for 500 000 cycles at the end. It can be  
172 observed that during the monotonic loading, the axial displacement increased quickly and it continued to  
173 increase during the cyclic loading, to reach 7.3 mm. The displacement was decreased to 6.8 mm when  
174 the load decreased from 100 kPa to 30 kPa.

175 Figure 6 shows the evolution of global displacement in *Unsaturated state* ( $w = 16\%$ ). The  
176 displacement increased quickly during the monotonic loading, from 0 to 7.3 mm. The pre-cyclic loading  
177 at 0.1 Hz, 1 Hz and 2 Hz increased the permanent displacement to 8.7 mm. The increasing rate of  
178 permanent displacement was also high in the first period of 5 Hz loading (from 8.7 mm to 9.9 mm for

179 the first 10 000 cycles) and then it slowed down (it needs nearly 50 000 cycles to increase from 9.9 mm  
180 to 10.9 mm).

181 Figure 7 depicts the evolution of permanent displacement during the 5 Hz loading. It shows that  
182 the displacement tended to increase linearly with the logarithm of cycle number  $N$  when  $N > 100$ . This is  
183 in agreement with the results of some previous studies. Indeed, in Paute and Le Fort (1984), Hornych  
184 (1993) and AFNOR (1995) for the unbound granular materials, the permanent displacement value at 100  
185 cycles was considered as the reference value in the modeling of ballast axial displacement after 100  
186 cycles. In these models, the displacement evolution varies also linearly with the loading cycle number  
187  $\log N$ .

188 From the image by the digital camera (Figure 8a), the movement of one ballast particle was  
189 monitored. The movement during *Unsaturated state* of this ballast particle was analyzed by considering  
190 the change in its contour (Figure 8b). It can be observed that there is not only vertical displacement but  
191 also horizontal one, indicating a rotation of the ballast particle. In general, the movements of other  
192 ballast particles follow the same trend. This suggests that ballast particles rearranged between  
193 themselves during the cyclic loading.

194 Figure 9 presents the evolution of volumetric water content (Figure 9a) and pore water pressure  
195 (Figure 9b) during the *Unsaturated state*. The initial volumetric water contents are  $\theta = 21.6\%$ ,  $22.7\%$   
196 and  $17.9\%$  at  $h = 120$  mm,  $160$  mm and  $200$  mm, respectively. Note that the  $200$  mm level corresponds  
197 to  $20$  mm below the ballast/sub-soil interface. As it was the last layer for the compaction operation, its  
198 dry unit mass can be smaller than those of lower layers.

199 As the sub-soil layer was fully saturated, the variation of volumetric water content  $\theta$  can be used  
200 to estimate its settlement by assuming that soil particles and water are not compressible.

201 The total height is divided into three sub-layers, assuming constant volumetric water content in each  
 202 sub-layer. The calculation of the settlement of each sub-layer is as follows:

$$\Delta V_{total} = h_1 \times A - \frac{V_{water}}{\theta_2}$$

$$\Delta h \times A = h_1 \times A - \frac{(h_1 \times A) \times \theta_1}{\theta_2} \quad (2)$$

$$\Delta h = h_1 \times \left( 1 - \frac{\theta_1}{\theta_2} \right)$$

204 where  $\Delta V_{total}$  and  $\Delta h$  are the variations of total volume and settlement of the sub-layer, respectively;  $\theta_1$   
 205 and  $\theta_2$  are respectively the volumetric water contents before and after the loading;  $V_{water}$  is the volume of  
 206 water in the sub-layer,  $A$  is the cross section of the specimen,  $h_1$  is the thickness of sub-layer before  
 207 loading.

208 The final settlement is the summary of the settlements of all sub-layers:

$$\Delta h = \Delta h_{120} + \Delta h_{160} + \Delta h_{200} \quad (3)$$

210 The settlement result obtained is also presented in Figure 6. It can be observed that the calculated  
 211 settlement has the same trend as the displacement by external measurement but slightly larger. Note that  
 212 the external displacement consists of both the displacements of ballast layer and sub-soil layer while the  
 213 calculated settlement consists of only the part of sub-soil. Note also that the accuracy of TDR used is 2%  
 214 that corresponds to a settlement of 4.3 mm.

215 During the 5 Hz loading for 500 000 cycles, the volumetric water content was almost stable with  
 216 small variations (Figure 9a). From the beginning to the end of the 5 Hz loading, the values are  $22.2 \pm$   
 217  $0.2\%$  for TDR1 at  $h = 120$  mm,  $23.4 \pm 0.3\%$  for TDR2 at  $h = 160$  mm and  $20.9 \pm 0.5\%$  for TDR3 at  $h =$

218 200 mm. On the whole, the degree of saturation of the whole sub-soil layer varied from 49% to 54%;  
219 this is quite close to the theoretical value of  $S_r$ , estimated at 55 %.

220 The response of tensiometers was plotted in Figure 9b. The curves of T1 ( $h = 120$ ) and T2 ( $h =$   
221 160) are very close while the curve of T3 ( $h = 200$ ) is clearly above. However, the shapes of the three  
222 curves are the same. After 20 h, the pore water pressure at all three levels reached their stabilization  
223 values: -166.4 kPa at  $h = 120$  mm; -163.9 kPa at  $h = 160$  mm and -114.1 kPa at  $h = 200$  mm.

224 For the visual monitoring, two photographs were taken, one before the monotonic loading and  
225 another after the 5Hz loading for 500 000 cycles, and they are presented in Figure 10a and Figure 10b,  
226 respectively. Referring to the level of the top surface of the sub-soil layer, these two photographs show  
227 that the level of ballast/sub-soil interface did not change. Furthermore, no migration of fine particles was  
228 observed. This suggests that the sub-soil displacement calculated from  $\theta$  does not represent the global  
229 variation. Note that the local ballast/sub-soil contact was not uniform over the whole interface section  
230 because ballast particles are very angular and have different shapes. This non-uniform contact can lead  
231 to non-uniform stress, thus a larger compression in the zones just beneath ballast particles as compared  
232 to the zones among particles. The TDR whose size is 80 mm long and 25 mm large was probably  
233 situated beneath ballast particles, giving rise to a higher  $\theta$  value, hence a larger estimated settlement.

234 When the 5 Hz loading for 500 000 cycles ended, the sample was connected to an external water  
235 source and water was observed on the ballast/sub-soil interface after about 1 day. During this time, the  
236 volumetric water content measured by TDR increased consistently: the value at  $h = 120$  mm changed  
237 firstly, then it was the turn of  $h = 160$  and finally of  $h = 200$  mm (Figure 11a). At  $t = 45$  h, the volumetric  
238 water contents at three levels stabilized. If one assumes that the dry unit mass of the sub-soil did not  
239 change during the test, the degree of saturation  $S_r$  was 87% to 88%. This is possible because during the  
240 saturation of very fine soil, it takes longtime to filling micro-pores. This can be observed also in Figure

241 11b where the evolution of pore water pressure is depicted. Till  $t = 45$  h, the pore water pressure  
242 increased as the volumetric water content increased. Afterwards, although the volumetric water content  $\theta$   
243 became stable, the pore water pressure continued to increase up to zero. Furthermore, the three pore  
244 water pressure-time curves show the same increase trend (Figure 11b), suggesting that the process of  
245 filling micro-pores took place continuously and uniformly within the sample.

246         Once all the tensiometers gave the positive pressure values, the third stage (*Saturated state*)  
247 started with the monotonic loading followed by the 5 Hz cyclic loading. Figure 12 shows the variations  
248 of the pressure applied (Figure 12a), the permanent axial displacement (Figure 12b), the pore water  
249 pressure (Figure 12c) and the volumetric water content (Figure 12d). When the monotonic load  
250 increased from 0 to 100 kPa, the permanent axial displacement increased from 9 mm to 28.6 mm, and  
251 the pore water pressure increased also: at  $h = 120$  mm and  $h = 200$  mm it increased quickly and reached  
252 around 30 kPa while at  $h = 0$  mm and  $h = 160$  mm it increases more gently. The gentle increase at  $h = 0$   
253 mm can be explained by the far distance of this position from the loading source and the low hydraulic  
254 conductivity of the soil, while the gentle increase at  $h = 160$  mm can be explained by some technical  
255 problem of the sensor at this level as revealed by the verification after the test. When the monotonic  
256 loading finished, the pore water pressure at all the three levels decreased but remained higher than zero.  
257 This can be explained by the very low hydraulic conductivity of the sub-soil that did not allow quick  
258 water pressure dissipation.

259         Under the 5 Hz loading, the permanent displacement continued to increase rapidly. The pore  
260 water pressure became quickly higher than 40 kPa (except the late response at  $h = 160$  mm, possibly due  
261 to the corresponding sensor performance). In the end, the value obtained was between 40 and 58 kPa.  
262 Note that the applied pressure varied from 30 kPa to 100 kPa. This suggests that the effective stress  
263 (total pressure minus pore pressure) became sometimes negative during the unloading (applied stress  
264 smaller than pore water pressure) and liquefaction occurred within the sub-soil. Note that the negative

265 value of effective stress has no-physical meaning; it implies simply that during unloading there were no  
266 longer contact between soil particles. Further study is needed to verify this point.

267 On one hand, the sharp increase of pore water pressure weakens the sub-soil and on the other  
268 hand its dissipation brings fine particles upward. This is the key factor for the migration of fine particles.  
269 This is also consistent with the observation reported by Aw (2007) and Indraratna et al. (2011): mud  
270 pumping was identified in the zone with presence of water which softens the base layer and allows the  
271 migration of the fine particles into the void spaces between ballast particles, and also the penetration of  
272 ballast particles into the sub-grade under loading. The penetration of ballast and the migration of fine  
273 particles created a layer of mixture materials. This is probably the main mechanisms for the creation of  
274 interlayer identified in some railway sub-structures in France as mentioned before. In Figure 12d, the  
275 change of volumetric water content is insignificant:  $\pm 1.4\%$  at  $h = 120$  mm,  $\pm 1.9\%$  at  $h = 160$  mm and  $\pm$   
276  $2.4\%$  at  $h = 200$  mm. Their variation trends are different: the volumetric water content at  $h = 120$  mm  
277 and  $160$  mm increased, while the value at  $h = 200$  mm decreased continuously. These trends can be  
278 explained as follows: assuming that the sub-soil is nearly saturated, when the soil was compressed, the  
279 pore volume decreased. As a result, the volumetric water content increased at  $h = 120$  mm and  $160$  mm.  
280 At  $h = 200$ , it is not very obvious because it was just  $20$  mm below the ballast/sub-soil interface that  
281 underwent significant modifications.

282 Figure 13 shows the photographs taken just before the monotonic loading (Figure 13a), after the  
283 monotonic loading (Figure 13b) and after the cyclic loading (Figure 13c) in *Saturated state*. The  
284 movement of fine particles can be identified. The fine particles were pumped up to the surface of ballast  
285 layer. During the monotonic loading, fine particles were also moving upwards, but not as rapidly as  
286 during the cyclic loading.

287 It can be seen that the fine particles migrated up to the ballast layer during the test (Figure 13).  
 288 For a further analysis, the evolution of the sub-soil surface from the initial surface (after compaction)  
 289 was recorded. From the images taken by camera (see Figure 13), the evolution of sub-soil surface was  
 290 monitored by digitization and the results are presented in Figure 14. The intersection between the initial  
 291 surface of sub-soil and the vertical ruler was chosen as the point zero in Figure 14. Each line represents  
 292 the level of sub-soil surface at one moment of the test. The time interval between lines is 2 minutes. The  
 293 first part (lower lines) corresponds to the variation during the monotonic loading and the second part  
 294 (higher lines) corresponds to the variation during the cyclic loading (5 Hz). In general, the entire sub-soil  
 295 surface was rising up. It is worth noting that when removing the sample at the end of the test, it was  
 296 observed that the pumping up level of fine particles was uniform over the whole cross section.

297 In order to verify the nature of fines migration, let's take an assumption that this was the ballast  
 298 penetration into the sub-soil that pushed the fine particle upward. In this way, a comparison between the  
 299 volume of ballast particles in sub-soil and the volume of ballast layer voids filled by fine particles up-  
 300 pumped was conducted. The volume occupied by ballast particles in sub-soil  $V_{ballast}$  is calculated as  
 301 follows:

$$302 \quad V_{ballast} = \frac{h_{ballast} \times A}{1 + e} \quad (4)$$

303 where  $h_{ballast}$  is the settlement of ballast layer,  $A$  is the sample cross section and  $e$  is the void ratio of  
 304 ballast layer.

305 The volume of ballast layer voids filled by fine particles of sub-soil  $V_{fines}$  can be calculated as follows:

$$306 \quad V_{fines} = \frac{h_{fines} \times A}{1 + e} e \quad (5)$$

307 where  $h_{fines}$  is the pumping up level of fine particles in the ballast layer. Admitting that ballast particles  
308 settlement pushed the fine sub-soil particles up and these fine particles fill the voids of ballast layer, i.e.,  
309  $V_{ballast} = V_{fines}$ . This leads to:

$$310 \quad h_{fines} = \frac{h_{ballast}}{e} \quad (6)$$

311 Indraratna et al. (1997) proposed that the voids ratio of ballast  $e$  can vary from 0.74 (compacted)  
312 to 0.95 (un-compacted). In the case of the present study, as the sample was submitted to the 5 Hz loading  
313 for 500 000 cycles, the ballast layer can be considered as compacted with a void ratio equal to 0.74. As  
314 the ballast settlement under loading in *Saturated state* is 47.7 mm as presented in Figure 12b ( the ballast  
315 settlement is considered equal to the piston displacement, the most critical case), the pumping up level  
316 estimated using Eq. (6) is 64.4. This value is much less than the real pumping up level of fine particles  
317 given in Figure 14:  $113.1 \pm 15$  mm. This suggests that there was not only the penetration of ballast  
318 particles pushing fine particles upwards, but also the dissipation of pore water pressure bringing fine  
319 particles up into the ballast layer, i.e. mud pumping occurred.

320 In order to have a better observation on the pumping up level of fine particles in the ballast layer,  
321 six reference vertical sections in Figure 14 (at the distances of 30 mm, 50 mm, 70 mm, 90 mm, 110 mm  
322 and 130 mm) were chosen. The evolutions of the sub-soil surface (pumping up levels) over time are  
323 determined and shown in Figure 15. This figure presents also the comparison between the real values of  
324 the sub-soil surface evolution with the theoretical value (Eq. 6). On the whole, the evolutions of the sub-  
325 soil surface at these sections follow the same trend. The interface rose up immediately when loading  
326 started. From Eq. (6), the theoretical pumping level of fine particles was calculated and the result is also  
327 presented in Figure 15. The calculated value is clearly lower than the real pumping level deduced from



328 the photographs. This confirms that the fine particles migration was not only due to the ballast  
329 penetration but also the dissipation of excess pore water pressure.

### 330 **Conclusions**

331 A physical model was developed to study the creation of interlayer and the mud-pumping phenomena in  
332 conventional railway sub-structure. The soil sample consisted of a ballast layer and one sub-soil layer.  
333 One pore water pressure sensor, three tensiometers, three TDRs were used to monitor the variations of  
334 pore water pressure and volumetric water content. The transparent PMMA apparatus wall and a digital  
335 camera allowed direct monitoring of the different movements (ballast, ballast/sub-soil interface, etc.). A  
336 test was carried out under monotonic and cyclic loading on a sample with the sub-soil in two different  
337 states: unsaturated and saturated states. The results obtained allowed the migration of fine particles to be  
338 investigated. The following conclusions can be drawn:

339 1) The quality of the recorded data showed that the physical model developed worked well and the test  
340 protocol adopted was appropriate. Moreover, it was observed that the migration of fine particles was  
341 globally the same in every points of the interface, suggesting that the soil sample was representative of  
342 the one dimensional case. Thereby, the experimental set-up developed and the test procedure adopted are  
343 relevant for studying the mud pumping phenomenon occurring in the railway substructure.

344 2) In the unsaturated state of sub-soil, the interface between two layers did not change even after the 5  
345 Hz loading for 500 000 cycles. On the contrary, in the near saturated state, it rose up very fast during the  
346 very first cycles. The difference between the two cases highlights the effect of water content which  
347 softens the base layer and allows the migration of the fine particles into the void spaces between ballast  
348 particles and also the penetration of ballast particles into the sub-grade.

349 3) The phenomenon produced in this test corresponds to the mud pumping phenomenon. The particle  
350 migration represents the intermixing between ballast and fine particles on one hand, and the fouling of  
351 railroad ballast by the underlying sub-soil on the other hand. The uniform pumping up level of fine  
352 particles confirms that the studied problem is one dimensional.

353 4) The mechanism behind the mud pumping phenomenon is the pore water pressure generation. Under  
354 cyclic loading, the pore water pressure can become higher than the total stress, giving rise to zero even  
355 negative effective stress. This is especially the case for the unloading phase. In this case, liquefaction  
356 occurs, that corresponds to the ideal condition for bring fine particles up under the effect of pore  
357 pressure dissipation. On the other hand, this is also the ideal condition for the penetration of ballast  
358 particles into the sub-soil, thus, for the interlayer creation. Note that the negative effective stress has no  
359 physical meaning; it implies simply that there were no longer any contact between soil particles and the  
360 unloading applied corresponded to a depression (suction) to water only. Further study is needed to verify  
361 this point.

## 362 **Acknowledgements**

363 This study was carried out within the research project “Reuse and reinforcement of conventional railway  
364 sub-structure and existing foundations”. The authors would like to address their deep thanks to Ecole des  
365 Ponts ParisTech (ENPC), Railway Network of France (RFF), French Railways Company (SNCF) and  
366 French National Research Agency for their supports.

## 367 **References**

368 AFNOR, 1995, “Essais Relatif aux Chaussées. Matériaux Non Traités. Part 1 : Essai Triaxial à  
369 Chargements Répétés, NF P98-235-1”, French Standard (In French).

370 AFNOR, 2004, “Unbound and hydraulically bound mixtures. Part 7: cyclic load triaxial test for unbound  
371 mixtures,” *French standard*, NF EN 13286-7.

372 Al Shaer, A., 2005, “Analyse des Déformations Permanentes des Voies Ferrées Ballastées – Approche  
373 Dynamique”, PhD Dissertation, Ecole Nationale des Ponts et Chaussées, France (In French).

374 Alobaidi, I. and Hoare, D.J., 1994, “Factors Affecting the Pumping of Fines at the Subgrade- Subbase  
375 Interface of Highway Pavements: A Laboratory Study”, *Geosynthetics International*, Vol. 1, No. 2, pp.  
376 221–259.

377 Alobaidi, I. and Hoare, D.J., 1996, “The Development of Pore Water Pressure at the Subgrade-Subbase  
378 Interface of a Highway Pavement and its Effect on Pumping of Fines”, *Geotextiles and Geomembranes*,  
379 Vol. 14, No. 2, pp. 111–135.

380 Alobaidi, I. and Hoare, D.J., 1998a, “Qualitative Criteria for Anti-pumping Geocomposites”, *Geotextiles  
381 and Geomembranes*, Vol. 16, No. 4, pp.221–245.

382 Alobaidi, I. and Hoare, D.J., 1998b, “The Role of Geotextile Reinforcement in the Control of Pumping  
383 at the Subgrade-Subbase Interface of Highway Pavements”, *Geosynthetics International*, Vol. 5, No. 6,  
384 pp. 619–636.

385 Alobaidi, I. and Hoare, D.J., 1999, “Mechanisms of Pumping at the Subgrade-Subbase Interface of  
386 Highway Pavements”, *Geosynthetics International*, Vol. 6, No. 4, pp. 241–259.

387 Aw, E.S., 2004, “Novel Monitoring System to Diagnose Rail Track Foundation Problems”, Master of  
388 Science Thesis, Massachusetts Institute of Technology, USA.

389 Aw, E.S., 2007, “Low Cost Monitoring System to Diagnose Problematic Rail Bed: Case Study at Mud  
390 Pumping Site”, Ph.D. Dissertation, Massachusetts Institute of Technology, USA.

391 Ayres, D.J., 1986, “Geotextiles or Geomembranes in Track? British Railway Experience”, *Geotextiles*  
392 *and Geomembranes*, Vol. 3, No. 2-3, pp. 129–142.

393 Burns, B., Ghataora, G.S. and Sharley, P., 2006, “Development and Testing of Geosand Composite  
394 Layers Using Pumps Index Test”, *In: Proceedings of the First International Conference on Railway*  
395 *Foundations Railfound06*, University of Birmingham, UK, pp. 355–366, ISBN10: 0-704426-00-5,  
396 ISBN13: 97807-04426-009.

397 Calon, N., Trinh, V.N., Tang, A.M., Cui, Y.J., Dupla, J.C., Canou, J., Lambert, L., Robinet, A. and  
398 Schoen O., 2010, “Caratérisation Hydraumécanique des Matériaux Constitutifs de Plateformes  
399 Ferroviaires Anciennes”. *Conférence JNGG2010*, Grenoble, France, p. 787–794 (In French).

400 Cui, Y. J. and Delage, P., 1996, “Yielding Behavior of an Unsaturated Compacted Silt”, *Géotechnique*  
401 Vol. 46, No. 2, pp. 291-311.

402 Cui, Y. J., Tang, A. M., Loiseau, C., and Delage, P., 2008, “Determining the Unsaturated Hydraulic  
403 Conductivity of a Compacted Sand-Bentonite Mixture Under Constant-Volume and Free-Swell  
404 Conditions”, *Physics and Chemistry of the Earth*, Parts A/B/C, Vol. 33, pp. S462–S471.

405 Cui, Y.J., Duong, T.V., Tang, A.M., Dupla, J.C., Calon, N. and Robinet, A., 2013, “Investigation of the  
406 Hydro-Mechanical Behaviour of Fouled Ballast”, *Journal of Zhejiang University- Science A*, Vol. 14,  
407 No.4, pp.244-255.

408 Duong, T.V., Trinh, V.N., Cui, Y.J., Tang, A.M. and Nicolas, C., 2013, “Development of a Large-Scale  
409 Infiltration Column for Studying the Hydraulic Conductivity of Unsaturated Fouled Ballast”,  
410 *Geotechnical Testing Journal*, Vol. 36, No. 1, pp. 54-63.

411 Ekblad, J., 2008, “Statistical evaluation of resilient models characterizing coarse granular materials,”  
412 *Materials and Structures*, Vol. 41, No. 3, pp. 509–525.

413 Ghataora, G.S., Burns, B., Burrow, M.P.N. and Evdorides, H.T., 2006, “Development of an Index Test  
414 for Assessing Anti-pumping Materials in Railway Track Foundations”, *In: Proceedings of the First*  
415 *International Conference on Railway Foundations, Railfound06*, University of Birmingham, UK, pp.  
416 355–366.

417 Hornych, P., Corté, J.F. and Paute, J.L., 1993, “Etude des Déformations Permanents sous Chargements  
418 Répétés de Trois Graves non Traitées”, *Bulletin de Liaison des Laboratoires des Ponts et Chaussées*,  
419 Vol.184, pp. 77-84 (In French).

420 Paute, J.L. and Le Fort, R., 1984, “Determination of Untreated Gravels Mechanical Characteristics with  
421 Cyclic Loading Triaxial Apparatus”, *Bulletin of the International Association of Engineering Geology*,  
422 No. 29, pp. 419 – 424, (In French).

423 Indraratna, B., Ionescu, D., Christie, D., and Chowdhury, R., 1997, “Compression and Degradation of  
424 Railway Ballast under One-dimensional Loading”, *Australian Geomechanics Journal*, Vol 12, pp. 48 –  
425 61.

426 Indraratna, B., Salim, W. and Rujikiatkamjorn. C., 2011, *Advanced Rail Geotechnology - Ballasted*  
427 *Track*. CRC Press.

428 Lackenby, J., Indraratna, B., Mcdowell, G., and Christie, D., 2007, “Effect of confining pressure on  
429 ballast degradation and deformation under cyclic triaxial loading,” *Géotechnique*, Vol. 57, No. 6, pp.  
430 527 – 536.

431 Lourenço, S.D.N., Gallipoli, D., Toll, D.G., Augarde, C.E. and Evans, F.D., 2011, “A New Procedure  
432 for the Determination of Soil-water Retention Curves by Continuous Drying Using High-suction  
433 Tensiometers”, *Canadian Geotechnical Journal*, Vol. 48, No. 2, pp. 327–335.

434 Mantho, A.T., 2005, “Echanges Sol-Atmosphère Application à la Sécheresse” Ph.D. Dissertation, Ecole  
435 Nationales des Ponts et Chaussées - Université Paris – Est, France (In French).

436 Raymond, G.P., “Railway Rehabilitation Geotextiles”, *Geotextiles and Geomembranes*, Vol. 17, No. 4,  
437 pp. 213–230.

438 Selig, E.T. and Waters, J.M., 1994, *Track Geotechnology and Substructure Management*. Thomas  
439 Telford.

440 SNCF, 1995, “Specification Technique pour la Fourniture des Granulats Utilisés pour la Réalisation et  
441 l’Entretien des Voies Ferrées ST 590B”, Technical guide (In French).

442 Takatoshi, I., 1997, “Measure for the stabilization of railway earth structure”, *Japan Railway Technical*  
443 *Service*.

444 Toll, D.G., Lourenço, S.D.N. and Mendes, J., 2012, “Advances in Suction Measurements Using High  
445 Suction Tensiometers”, *Engineering Geology*, doi:10.1016/j.enggeo.2012.04.013.

446 Topp, G.C., Davis, J.L. and Annan, A.P., 1980, “Electromagnetic Determination of Soil Water Content:  
447 Measurements in Coaxial Transmission Lines”, *Water Resources Research*, Vol. 16, No. 3, pp. 574–582.

448 Trinh, V.N., 2011, “Comportement Hydromécanique des Matériaux Constitutifs de Plateformes  
449 Ferroviaires Anciennes”. Ph.D. Dissertation, Ecole Nationales des Ponts et Chaussées - Université Paris  
450 – Est, France (In French).

451 Trinh, V.N., Tang, A.M., Cui, Y.J., Canou, J., Dupla, J.C., Calon, N., Lambert, L., Robinet, A. and  
452 Schoen, O., 2011, “Caractérisation des Matériaux Constitutifs de Plate-forme Ferroviaire Ancienne”,  
453 *Revue Française de Géotechnique*, Vol. 134-135, pp. 65–74 (In French).

454 Trinh, V.N., Tang, A.M., Cui, Y.J., Dupla, J.C., Canou, J., Calon, N., Lambert, L., Robinet, A. and  
455 Schoen, O., 2012, “Mechanical Characterisation of the Fouled Ballast in Ancient Railway Track Sub-  
456 structure by Large-scale Triaxial Tests”, *Soils and Foundations*, Vol. 52, No. 3, pp. 511-523.

457 Van, W. A., 1985, “Rigid Pavement Pumping: (1) Subbase Erosion and (2) Economic Modeling :  
458 Informational Report”, *Publication FHWA/IN/JHRP-85/10. Joint Highway Research Project*, Indiana  
459 Department of Transportation and Purdue University, West Lafayette, Indiana, USA,  
460 doi:10.5703/1288284314094

461 Yasuda, N., Matsumoto, N., Yoshioka, R., and Takahashi, M., 1997, “Undrained monotonic and cyclic  
462 strength of compacted rockfill material from triaxial and torsional simple shear tests,” *Canadian*  
463 *Geotechnical Journal*, Vol. 34, No. 3, pp. 357-367.

464 Yoder, E.J., 1957, “Pumping of Highway and Airfield Pavements: Technical Paper”, *Publication*  
465 *FHWA/IN/JHRP-57/05. Joint Highway Research Project*, Indiana Department of Transportation and  
466 Purdue University, West Lafayette, Indiana, doi: 10.5703/1288284313518.

467 Yuan, R., Yang, Y.S., Qiu, X. and Ma, F.S., 2007, “Environmental Hazard Analysis and Effective  
468 Remediation of Highway Seepage”, *Journal of Hazardous Materials*, Vol. 142, No. 1-2, pp. 381–388.

469 Zhang, C., 2004, “The Effect of High Groundwater Level on Pavement Sub-grade Performance”, Ph.D.  
470 Dissertation, the Florida State University - College of Engineering, USA.

471	List of Tables
472	Table 1: Characteristic of sub-soil <i>70S30K</i>
473	List of Figures
474	Figure 1: Grain size distribution curve of studied material
475	Figure 2: Normal proctor curve of the sub-soil
476	Figure 3: Schematic view of the apparatus
477	Figure 4: Photograph of the physical model
478	Figure 5: Pre-loading in <i>Unsaturated state</i>
479	Figure 6: Axial displacement during loading in <i>Unsaturated state</i>
480	Figure 7: Displacement during cyclic loading at 5 Hz in <i>Unsaturated state</i>
481	Figure 8: Monitoring of one ballast particle movement
482	Figure 9: Changes in volumetric water content and pore water pressure in <i>Unsaturated state</i>
483	Figure 10: Photographs of the interface between two soils layers: a) before and b) after loading in
484	<i>Unsaturated state</i>
485	Figure 11: Changes in volumetric water content and pore water pressure during <i>Saturation</i>
486	Figure 12: Test on the sub-soil at <i>Saturated state</i> : a) applied pressure; b) permanent axial displacement;
487	c) pore water pressure and d) volumetric water content
488	Figure 13: Photographs showing the evolution of interface between two the soils layers: fine particles
489	were pumped upwards
490	Figure 14: Sub-grade surface evolution
491	Figure 15: Pumping level of fine particles during the test in <i>Saturated state</i>

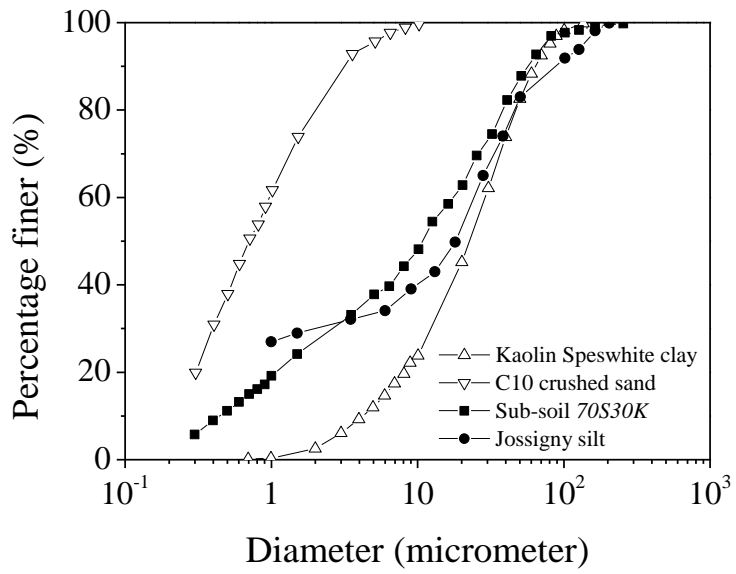


492

493 **Table 1: Properties of sub-soil 70S30K**

Specific gravity of clay $G_s$	2.6
Specific gravity of crushed sand $G_s$	2.65
Initial dry unit mass $\rho_d$	1.5 Mg/m <sup>3</sup>
Porosity $n$	43%
Liquid Limit $LL$	27%
Plasticity Index $IP$	11%
Hydraulic conductivity $K$ ( $\rho_d = 1.5 \text{ Mg/m}^3$ )	$8.4 \times 10^{-7} \text{ m/s}$
Optimum water content $w$	16%

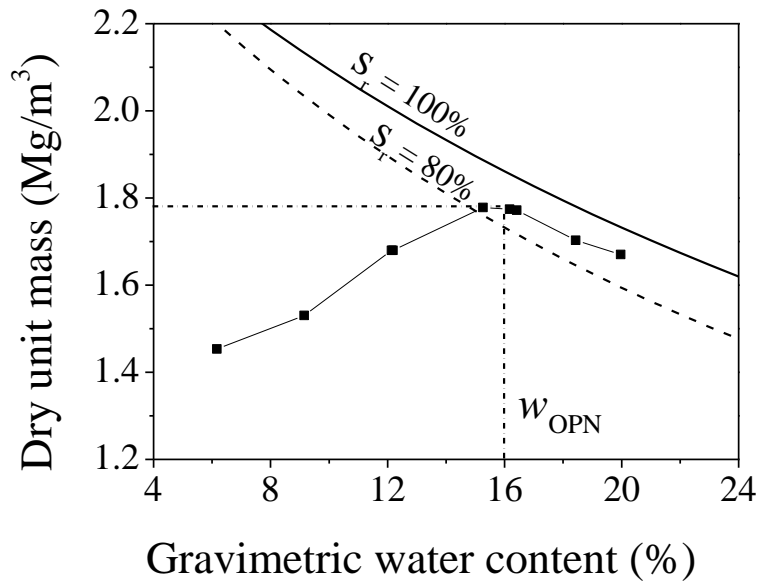
494



495

496 **Figure 1: Grain size distribution curve of studied material**

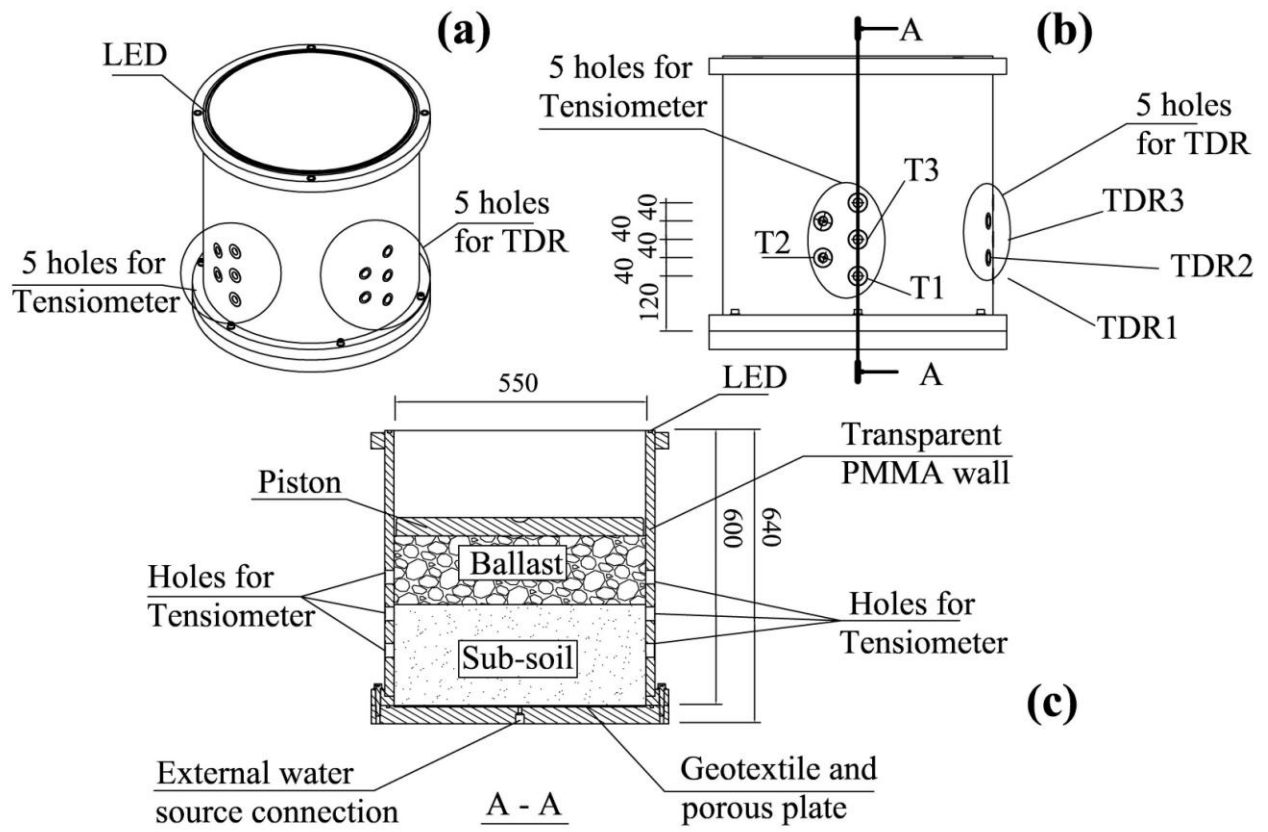
497



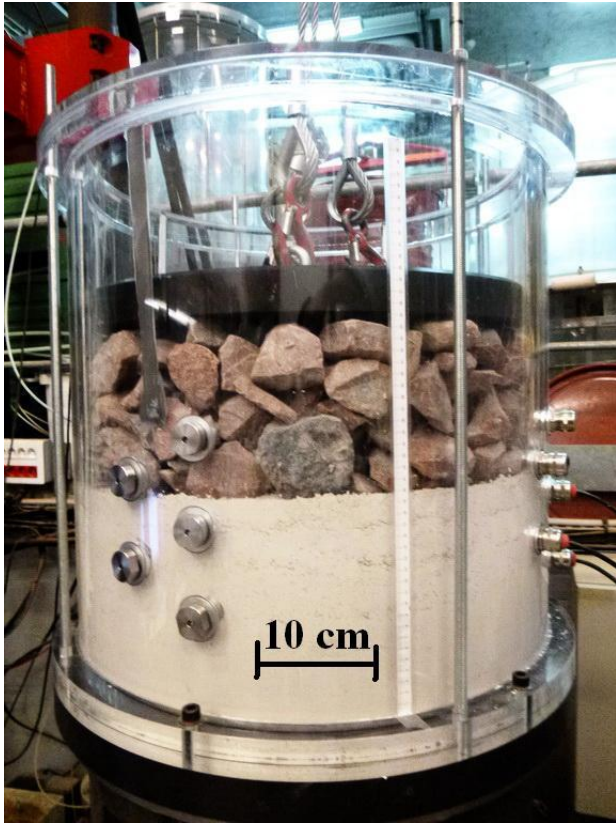
498

499 **Figure 2: Normal proctor curve of the sub-soil**

500



501  
 502 **Figure 3: Schematic view of the apparatus**

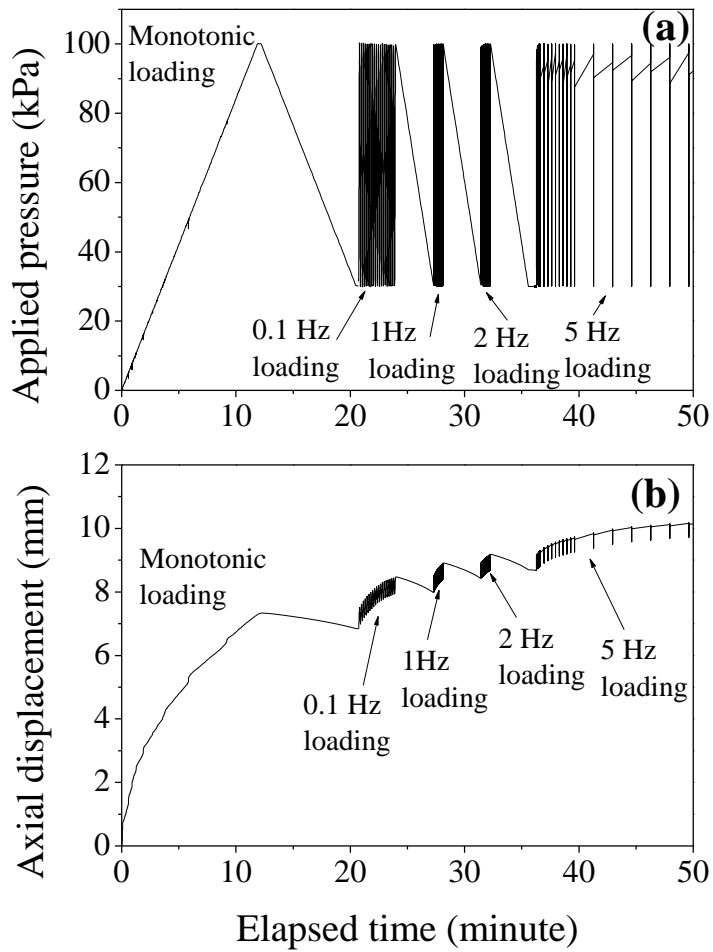


503

504 **Figure 4: Photograph of the physical model**

505

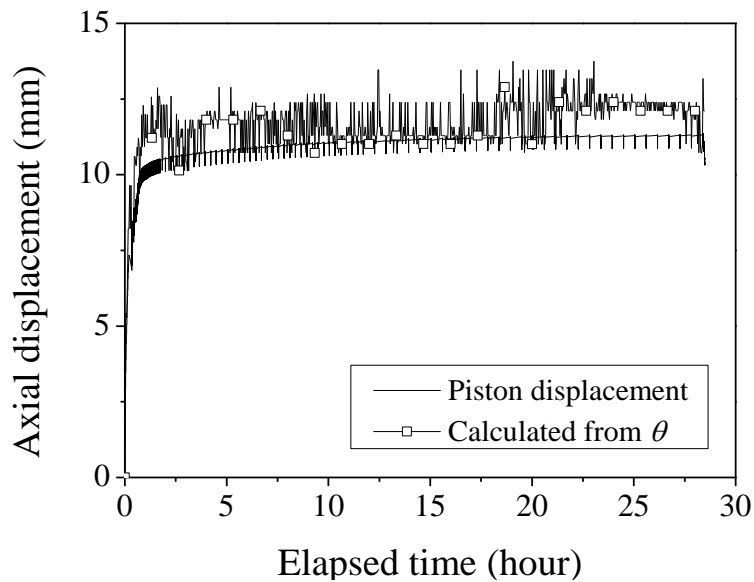
506



507

508

Figure 5: Pre-loading in *Unsaturated state*

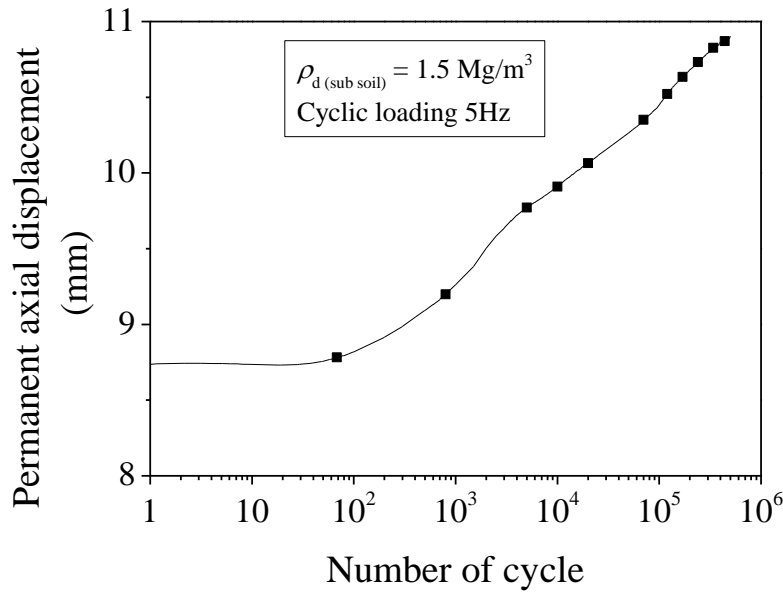


509

510

Figure 6: Axial displacement during loading in *Unsaturated state*

511  
512  
513



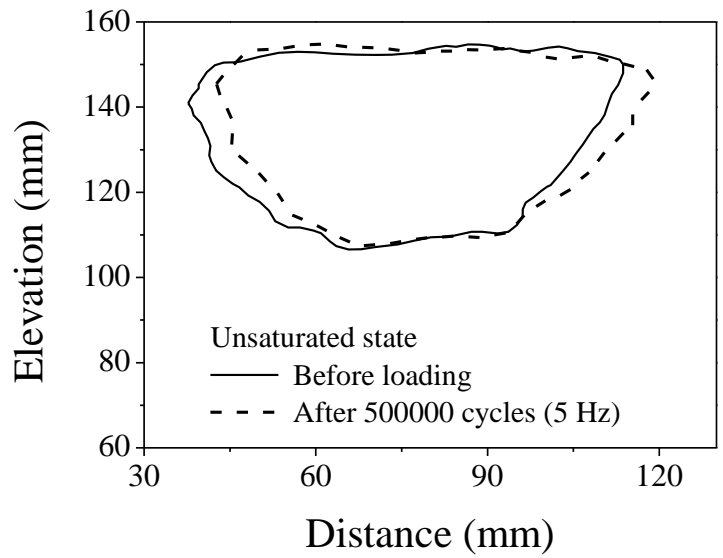
514  
515  
516

517 **Figure 7: Displacement during cyclic loading at 5 Hz in *Unsaturated state***

518



a) Reference ballast particle

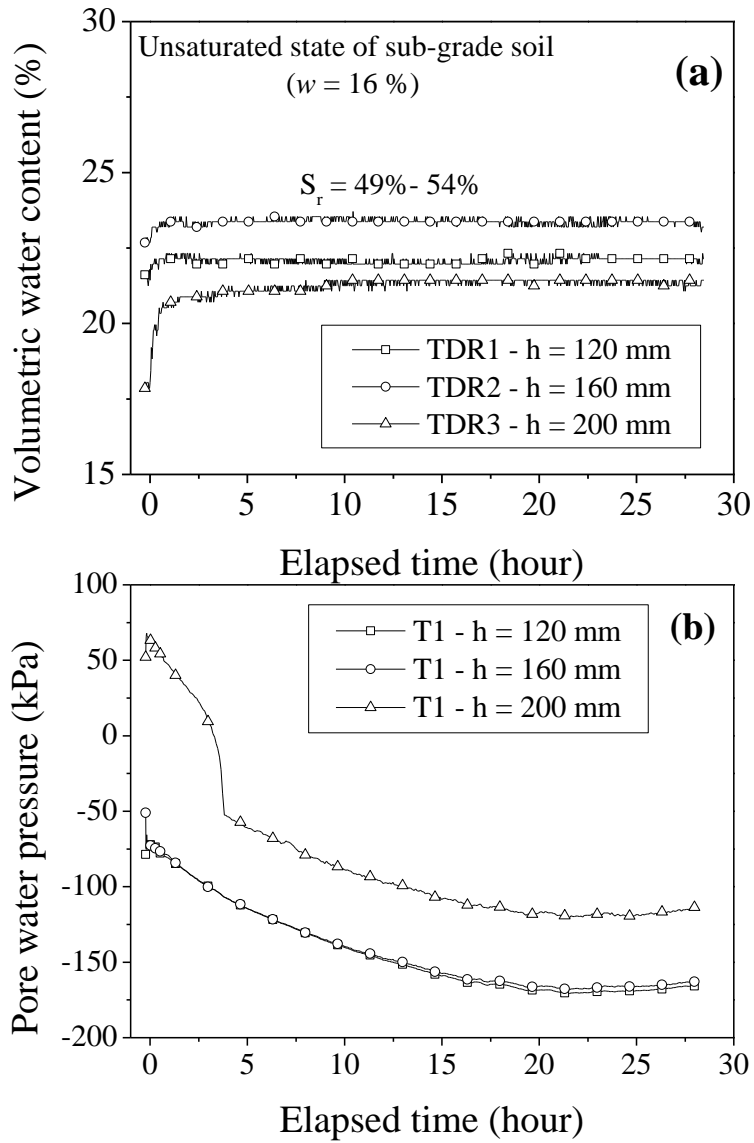


b) Outline ballast change before and after loading in *Unsaturated state*

519

520 **Figure 8: Monitoring of one ballast particle movement**

521  
522  
523



524  
525

Figure 9: Changes in volumetric water content and pore water pressure in *Unsaturation state*



a) Before loading ( $w = 16\%$ )

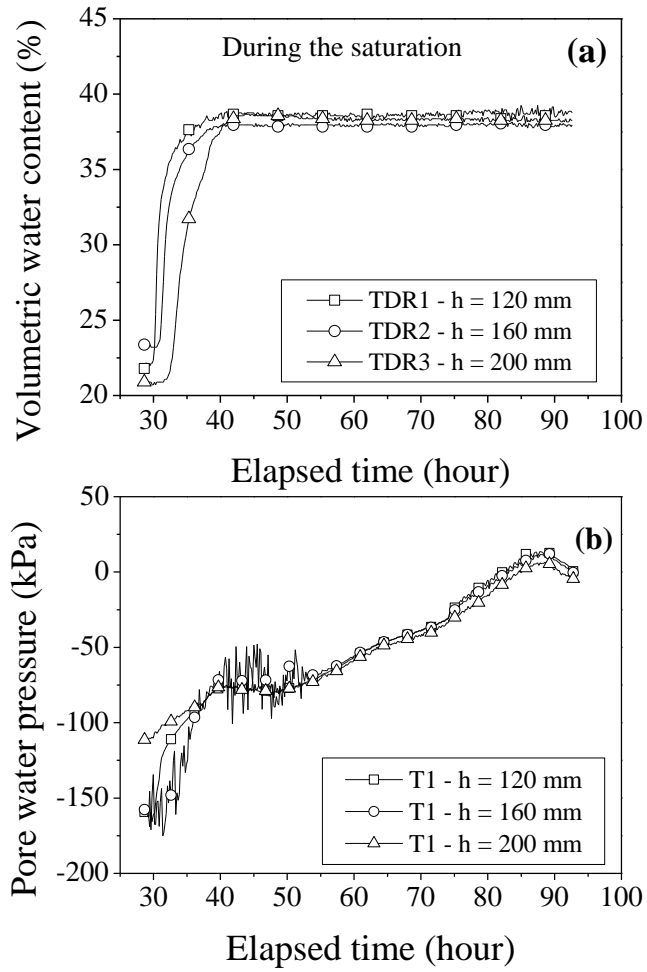


b) After loading ( $w = 16\%$ )

526 **Figure 10: Photographs of the interface between two soils layers: a) before and b) after loading in *Unsaturated state***

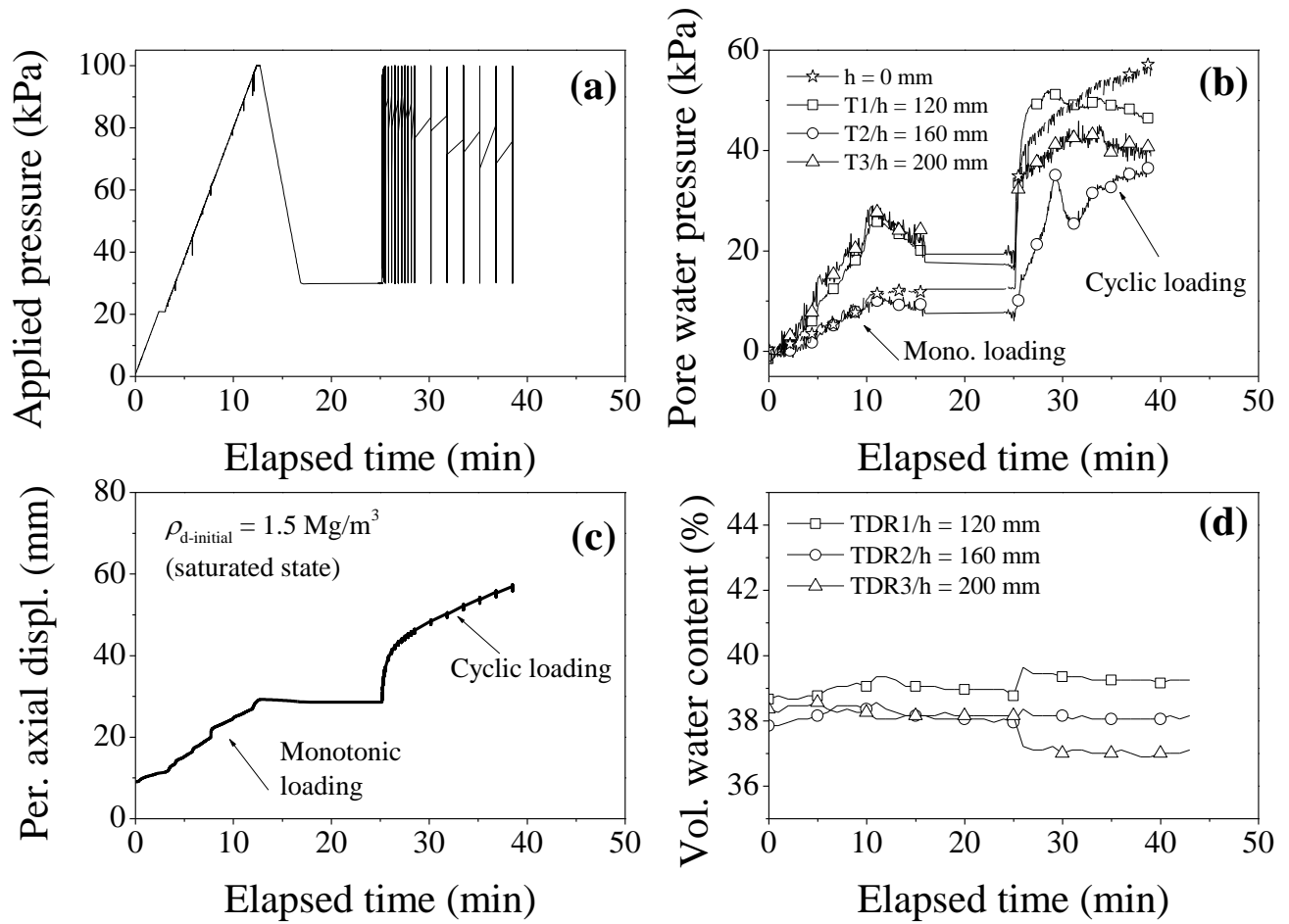


527  
528



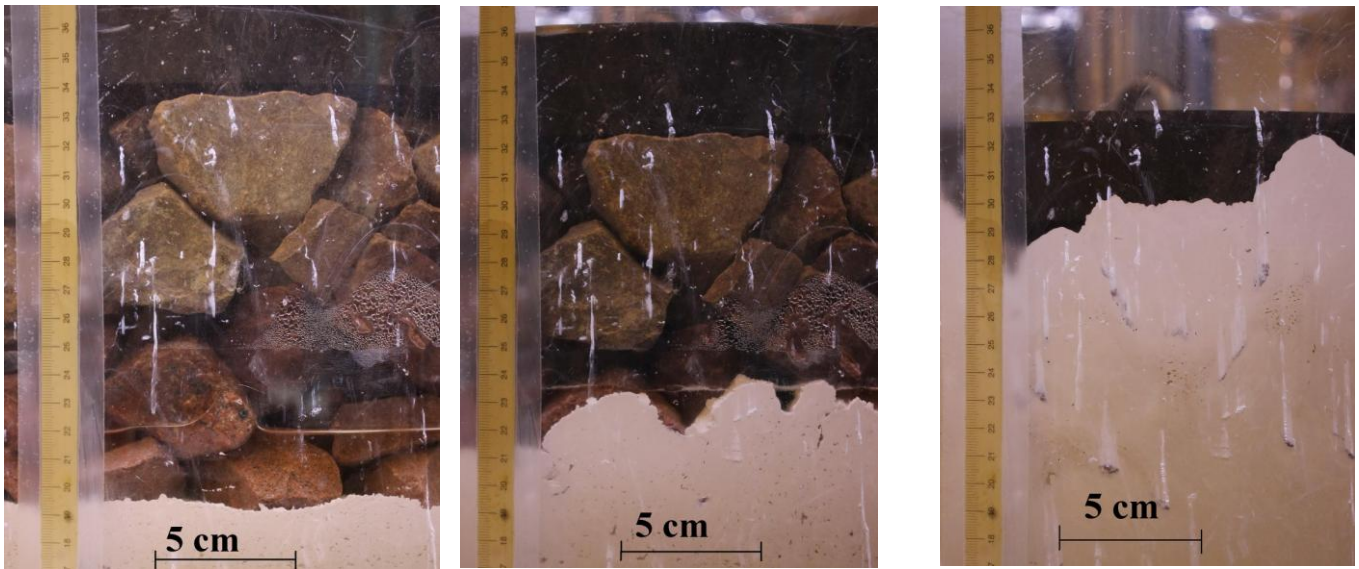
529  
530  
531

Figure 11: Changes in volumetric water content and pore water pressure during Saturation



532  
 533 **Figure 12: Test on the sub-soil at *Saturated state*: a) applied pressure; b) permanent axial displacement; c) pore water**  
 534 **pressure and d) volumetric water content**

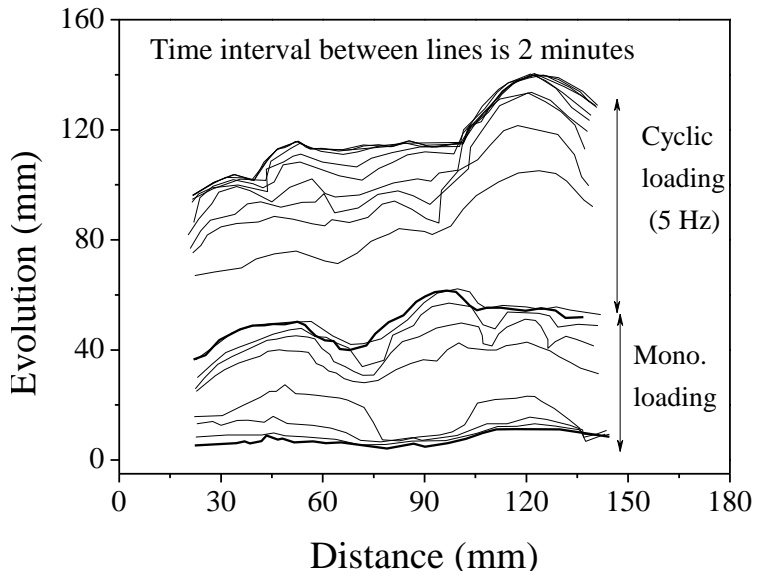
535  
 536  
 537  
 538  
 539  
 540



a) after saturation and before monotonic loading      b) after monotonic loading (saturated state)      c) after cyclic loading (saturated state)

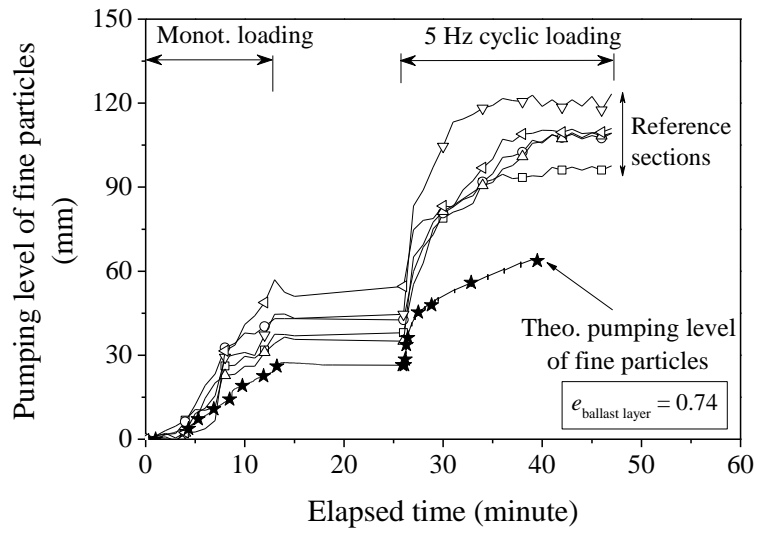
541 **Figure 13: Photographs showing the evolution of interface between two the soils layers: fine particles were pumped**  
 542 **upwards**

543  
 544  
 545  
 546  
 547



548 **Figure 14: Sub-grade surface evolution**  
 549

550



551

552 **Figure 15: Pumping level of fine particles during the test in *Saturated state***

553